This is a repository copy of *Cycling chaotic attractors in two models for dynamics with invariant subspaces*.

White Rose Research Online URL for this paper:
http://eprints.whiterose.ac.uk/1001/

Citation for the published paper
Ashwin, P. and Rucklidge, A.M. and Sturman, R. (2004) *Cycling chaotic attractors in two models for dynamics with invariant subspaces.* Chaos: An Interdisciplinary Journal of Nonlinear Science, 14 (3). pp. 571-582.

Citation for this paper
To refer to the repository paper, the following format may be used:

Ashwin, P. and Rucklidge, A.M. and Sturman, R. (2004) *Cycling chaotic attractors in two models for dynamics with invariant subspaces.*
Author manuscript available at: http://eprints.whiterose.ac.uk/archive/00001001/
[Accessed: *date*].
Published in final edited form as:

Ashwin, P. and Rucklidge, A.M. and Sturman, R. (2004) *Cycling chaotic attractors in two models for dynamics with invariant subspaces.* Chaos: An Interdisciplinary Journal of Nonlinear Science, 14 (3). pp. 571-582.

Cycling chaotic attractors in two models for dynamics with invariant subspaces

Peter Ashwin[*]

Department of Mathematical Sciences, Laver Building,
University of Exeter, Exeter EX4 4QE, UK

Alastair M. Rucklidge[†]and Rob Sturman[‡][§]
Department of Applied Mathematics, University of Leeds,
Leeds LS2 9JT, UK

May 17, 2004

Abstract

Nonergodic attractors can robustly appear in symmetric systems as structurally stable cycles between saddle-type invariant sets. These saddles may be chaotic giving rise to 'cycling chaos'. The robustness of such attractors appears by virtue of the fact that the connections are robust within some invariant subspace. We consider two previously studied examples and examine these in detail for a number of effects: (i) presence of internal symmetries within the chaotic saddles, (ii) phase-resetting, where only a limited set of connecting trajectories between saddles are possible and (iii) multistability of periodic orbits near bifurcation to cycling attractors.

The first model consists of three cyclically coupled Lorenz equations and was investigated first by Dellnitz *et al.* (1995). We show that one can find a 'false phase-resetting' effect here due to the presence of a skew product structure for the dynamics in an invariant subspace; we verify this by considering a more general bi-directional coupling. The presence of internal symmetries of the chaotic saddles means that the set of connections can never be clean in this system, that is, there will always be transversely repelling orbits within the saddles that are transversely attracting on average. Nonetheless we argue that 'anomalous connections' are rare.

The second model we consider is an approximate return mapping near the stable manifold of a saddle in a cycling attractor from a magnetoconvection problem previously investigated by two of the authors. Near resonance, we show that the model genuinely is phase-resetting, and there are indeed stable periodic orbits of arbitrarily long period close to resonance, as previously conjectured. We examine the set of nearby periodic orbits in both parameter and phase space and show that their structure appears to be much more complicated than previously suspected.

[*]P.Ashwin@ex.ac.uk

[†]A.M.Rucklidge@leeds.ac.uk

[‡]R.Sturman@bristol.ac.uk

[§]Current address: Department of Mathematics, University of Bristol, University Walk, Bristol, BS8 1TW, UK

In particular, the basins of attraction of the periodic orbits appear to be *pseudo-riddled* in the terminology of Lai (2001).

1 Introduction

Robust heteroclinic attractors between saddle-type equilibria or periodic orbits have been observed to arise as attractors in a number of systems, both theoretically and in practical models. More recently, it has been noticed that robust heteroclinic attractors may appear between saddles that are chaotic: so-called *cycling chaos* [1, 7, 8]. However there is still a poor understanding of the dynamics of such attractors due to the fact that the chaotic dynamics on the invariant subspace may lead to a variety of transverse behaviors of trajectories and indeed considerable difficulties for performing qualitatively accurate numerics. In this paper we focus on identifying some new phenomena in existing examples of cycling chaos. This includes the appearance of phase-resetting, anomalous connections caused by the presence of points of higher symmetry within the saddles and resonance bifurcations of these attractors to form periodic orbits.

In [7] cycling chaos was considered for three Lorenz-type systems coupled in a ring. This system was found to have attractors that consist of heteroclinic cycles between three symmetry-related chaotic saddles, each of which is a Lorenz attractor within the three-dimensional invariant subspace such that the other two systems are fixed at the origin. The chaotic saddles in [7] are not isolated from each other: they contain a common equilibrium at the origin. This means that they cannot be modeled in the usual analogy with a heteroclinic cycle between equilibria and there are *anomalous connections* between the chaotic saddles caused by close approaches to the origin. These have previously been not permitted in analyses of cycling chaos: see for example [1, 8]. However, this is a manifestation of a more general phenomenon: chaotic saddles in symmetric systems can (and often do) contain points with more symmetry than typical points within the saddle, i.e., points with higher isotropy. These higher isotropy points may be unstable fixed points or equilibria (as in the case for the Lorenz system) or even chaotic saddles (as in the case of a chaotic attractor that is 'stuck on' to an invariant subspace. In either case the presence of higher isotropy points leads to a complication in the structure of the chaotic saddle and prevents the possibility of choosing a global section to the connections.

One aspect we investigate is the effect of points of higher isotropy; in fact we argue in Section 2.3 that anomalous connections will typically not appear within the attractor even when they are present. This means that, at least for the systems considered, the presence of points with higher isotropy in the chaotic saddles do not seem to disturb the order of visiting the chaotic saddles except in exceptional cases.

Another dynamical effect that can appear in cycling chaos is that of *phase-resetting connections* [3] or *selection of connections* [4]. In those papers phase-resetting connections appeared due to

the presence of a saddle equilibrium with a one-dimensional unstable manifold as a node of the heteroclinic cycle. We were surprised to find a similar effect for the model of [7] even though each node is a fully chaotic attractor and hence the set of connections between adjacent saddles must have dimension strictly larger than one. We resolve this paradox by noting that the phase-resetting effect is simply because the chosen form of coupling (unidirectional) gives a skew-product factorization of the system within the subspace containing the connections. On including more general bi-directional coupling, this phase-resetting disappears. We call this effect *false phase-resetting*.

A final aspect of these attractors that we consider in this paper is the creation of cycling attractors at resonance bifurcations. As noted in [2, 3, 4], this bifurcation seems to be associated with the appearance of a very large number of stable periodic orbits that shadow the orbits within the cycling chaos. We show that this effect also appears to be present in both models we consider, and moreover the structure of the basins of attraction of the resulting stable periodic orbits appear to be pseudo-riddled [10].

The paper is structured as follows: in Section 2 we examine an example introduced by Dellnitz *et al.* in [7] of three cyclically coupled Lorenz attractors. We characterize the rate of attraction to the cycling attractor by means of transverse Lyapunov exponents along the lines of [1]. We illustrate that the presence of points of higher isotropy does not typically result in any major changes in observed numerical behavior; however, it does mean that the footprint of transverse Lyapunov exponents as considered in [1] always shows totally unstable measures within the saddle and complicates the geometry of the connections. For this example we can obtain a simple characterization of the footprint, discuss the appearance of false phase-resetting and the absence of anomalous connections. In Section 3 we return to a map derived as a low dimensional model of a magnetoconvection problem in [2]. Near a resonance of the cycling attractor, we find that the basin of attraction of the periodic orbits have a complicated pseudo-riddled structure. We demonstrate how one can estimate the location of periodic orbits near resonance for this map. In the final discussion section we remark on some aspects of the classification of general attractors of the type investigated here.

2   Three cycling Lorenz attractors

We consider a system of three coupled Lorenz systems which is a slight generalization of the system studied in [7]:

$$
\begin{aligned}
\dot{\mathbf{x}}_1 &= g(\mathbf{x}_1) + h(\mathbf{x}_1, \mathbf{x}_2, \mathbf{x}_3), \\
\dot{\mathbf{x}}_2 &= g(\mathbf{x}_2) + h(\mathbf{x}_2, \mathbf{x}_3, \mathbf{x}_1), \\
\dot{\mathbf{x}}_3 &= g(\mathbf{x}_3) + h(\mathbf{x}_3, \mathbf{x}_1, \mathbf{x}_2),
\end{aligned}
\tag{1}
$$

where $\mathbf{x}_j \in \mathbb{R}^3$. We write $\mathbf{x}_i = (x_i, y_i, z_i)$ then we assume that each cell has Lorenz dynamics in the absence of coupling given by

$$g(x, y, z) = (\sigma(y - x), Rx - y - xz, -\beta z + xy), \tag{2}$$

with $\sigma = 15$, $R = 58$ and $\beta = 2.4$ and we set the coupling between cells to be

$$h(\mathbf{x}_1, \mathbf{x}_2, \mathbf{x}_3) = \gamma |\mathbf{x}_2|^2 \mathbf{x}_1 + \nu |\mathbf{x}_3|^2 \mathbf{x}_1, \tag{3}$$

meaning that there is a coupling of strength γ from i to $i-1$ and one of strength ν from i to $i+1$. This system has a symmetry of the form

$$\Phi(\mathbf{x}_1, \mathbf{x}_2, \mathbf{x}_3) = (\mathbf{x}_2, \mathbf{x}_3, \mathbf{x}_1)$$

and has internal (local) symmetries of the form $\kappa_{1,2,3}$ where

$$\kappa_1(\mathbf{x}_1, \mathbf{x}_2, \mathbf{x}_3) = (-x_1, -y_1, z_1, \mathbf{x}_2, \mathbf{x}_3)$$

and similarly for $\kappa_{2,3}$. The symmetries of the system force the invariance of some subspaces as in Figure 1. Note that the coordinate planes ($P_{12} = (\mathbf{x}_1, \mathbf{x}_2, 0)$ etc.) and axes ($L_1 = (\mathbf{x}_1, 0, 0)$ etc.) are invariant, and are subsets of the invariant subspaces given in the table ($P_{ij} \subset N_{ij}$ and $L_i \subset S_i$). However the invariance of these subspaces is due to the form of the dynamics (a fixed point at the origin) rather than just a symmetry.

On the invariant subspace P_{12} the dynamics reduces to the six-dimensional system

$$\dot{\mathbf{x}}_1 = g(\mathbf{x}_1) + \gamma |\mathbf{x}_2|^2 \mathbf{x}_1$$
$$\dot{\mathbf{x}}_2 = g(\mathbf{x}_2) + \nu |\mathbf{x}_2|^2 \mathbf{x}_2$$

and so in particular when $\nu = 0$ (as in [7]) the dynamics is a skew product over the dynamics within S_2. An effect of this is that although there are many trajectories from a saddle in S_1 to one in S_2 they all project to the same trajectory within S_2. As a result the dynamics projected onto S_2 appears to be phase resetting although in the sense of [4] it is not. In other words, the case $\nu = 0$ is degenerate for the dynamics of a system with this symmetry.
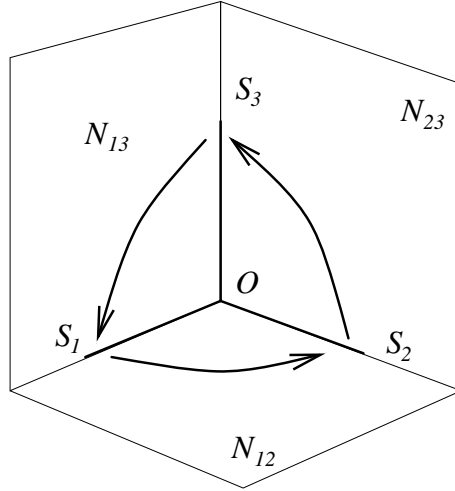
We first reproduce in Figure 2(a) the results of [7] for $\nu = 0$, choosing $\gamma = -0.014$ such that $\rho = 1.1135 > 1$ in (6). Here we have an attracting heteroclinic cycle between chaotic saddles, with cycling chaos characterized by a slowing down of the trajectory around the cycle. The cycling attractor consists of chaotic attractors A_i for the system restricted to the subspaces S_i and connecting orbits. For a different value of $\gamma = -0.012$, we obtain a periodic orbit (Figure 2(b)), demonstrating the resetting nature of the connection between the chaotic sets.

2.1 Transverse Lyapunov exponents and the footprint for chaotic saddles

In the absence of any coupling ($\gamma = \nu = 0$) the transverse Lyapunov exponents for the saddles $A_i \subset L_i \subset S_i$ are easy to compute. In both the N_{12} and N_{13} directions the most positive exponent

4

Name	Subspace	Symmetry generators
S_1	$(\mathbf{x}_1, 0, 0, z_2, 0, 0, z_3)$	κ_2, κ_3
S_2	$(0, 0, z_1, \mathbf{x}_2, 0, 0, z_3)$	κ_1, κ_3
S_3	$(0, 0, z_1, 0, 0, z_2, \mathbf{x}_3)$	κ_1, κ_2
N_{12}	$(\mathbf{x}_1, \mathbf{x}_2, 0, 0, z_3)$	κ_3
N_{23}	$(0, 0, z_1, \mathbf{x}_2, \mathbf{x}_3)$	κ_1
N_{13}	$(\mathbf{x}_1, 0, 0, z_2, \mathbf{x}_3)$	κ_2
P	$(\mathbf{x}, \mathbf{x}, \mathbf{x})$	Φ
O	$(0, 0, z_1, 0, 0, z_2, 0, 0, z_3)$	$\kappa_1, \kappa_2, \kappa_3$

(a)

(b)

Figure 1: (a) Table of invariant subspaces and (b) schematic illustration of the invariant subspaces of the system of three coupled Lorenz systems with cycling attractors. The chaotic saddles A_i (denoted by thick lines) are within the S_i and intersect at the origin within O.
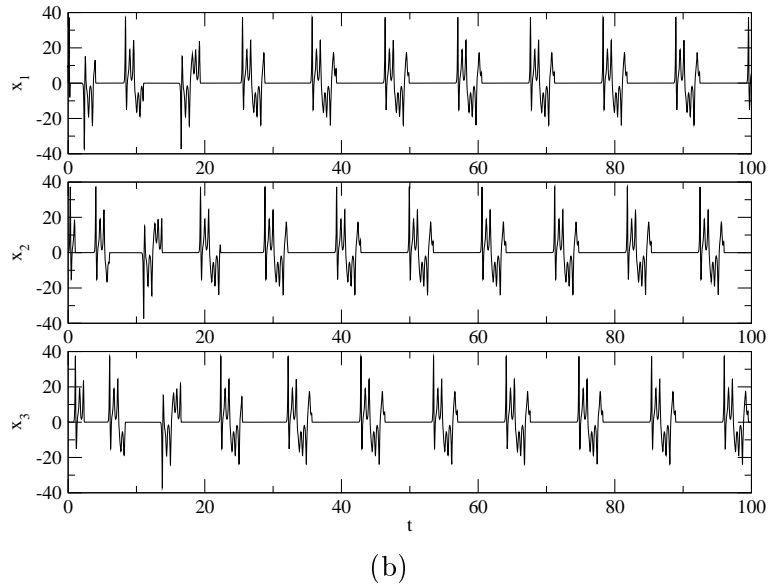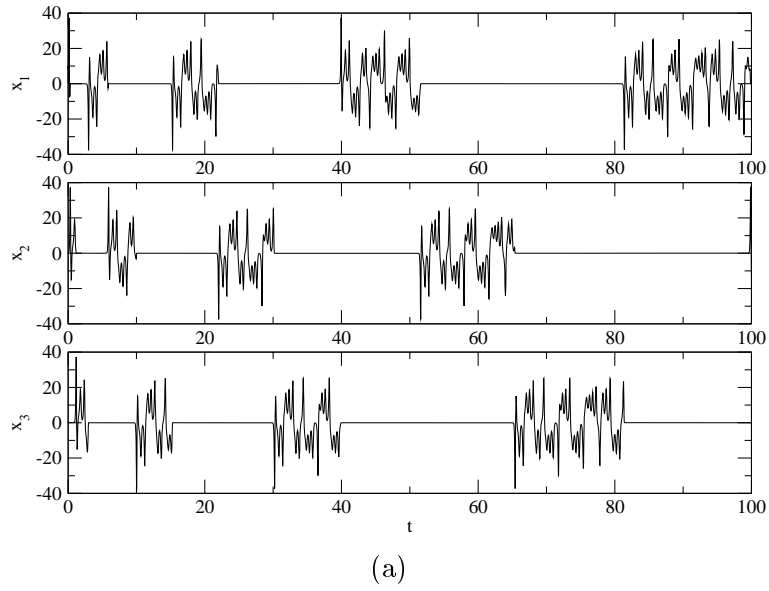
Figure 2: Timeseries for trajectories of the system (1) for coupled Lorenz systems, with $\nu = 0$. In (a) $\gamma = -0.014$ and we observe slowing down cycling chaos as in [7] whereas in (b) $\gamma = -0.012$ there is an approximately periodic orbit with period around 11 that is observed as an attractor.

6

for the origin is the most positive eigenvalue of

$$Dg(\mathbf{0}) = \begin{pmatrix} -\sigma & \sigma \\ R & -1 \end{pmatrix}$$

namely, for the parameters $\sigma = 15$, $R = 58$, $\beta = 2.4$ used by [7] and ourselves throughout this section, we have $\tilde{\lambda}_{12} = \tilde{\lambda}_{13} = 22.31501$. We exploit the special structure of the coupling by h to give an explicit formula for the largest Lyapunov exponents given any ergodic invariant measure μ supported in S_1. This is

$$\begin{aligned}
\lambda_{13} &= \tilde{\lambda}_{13} + \gamma \int |\mathbf{x}|^2 \, d\mu(\mathbf{x}), \\
\lambda_{12} &= \tilde{\lambda}_{12} + \nu \int |\mathbf{x}|^2 \, d\mu(\mathbf{x}).
\end{aligned} \tag{4}$$

In order to verify this, firstly note that the linearization transverse at $(\mathbf{x}_1, 0, 0) \in S_1$ in the direction N_{13} is given by the linear cocycle

$$\dot{\mathbf{y}} = \left(Dg(\mathbf{0}) + \gamma |\mathbf{x}_1|^2\right) \mathbf{y}. \tag{5}$$

We claim that the most unstable direction is simply given by the eigenvector $\mathbf{e}$ corresponding to the most unstable eigenvalue of $Dg(\mathbf{0})$. To see this, note that any solution of (5) has the form $\mathbf{y}(t) = e^{a(t)} \mathbf{z}(t)$ where $\dot{a} = \gamma |\mathbf{x}_1|^2$ and $\mathbf{z}$ satisfies $\dot{\mathbf{z}} = Dg(0)\mathbf{z}$. Hence the most unstable direction for (5) is given by $\mathbf{e}$ and the Lyapunov exponent in this direction is $\lambda_{13} = \tilde{\lambda} + \gamma \langle |\mathbf{x}_1|^2 \rangle$. Applying the ergodic theorem for the measure μ (and the same argument for λ_{12}) gives (4).

The form of the equations (4) means one can easily compute $(\lambda_{12}(\mu), \lambda_{13}(\mu))$ for any measure μ in the set of ergodic measures supported on the chaotic saddle A_1 in S_1. The set of points obtained was termed the *footprint* of transverse Lyapunov exponents in [1] and this can be used to characterize the attractiveness or otherwise of the heteroclinic cycle. We say an ergodic measure μ undergoes a resonance bifurcation when $\lambda_{13}(\mu)/\lambda_{12}(\mu) = -1$. By (4) this means that in (γ, ν)-parameter space the resonance bifurcation occurs where $\gamma + \nu = -2\tilde{\lambda}/\langle |\mathbf{x}^2| \rangle$. If we write

$$\rho = |\lambda_{12}/\lambda_{13}| \tag{6}$$

then the cycling is attracting in the case $\rho > 1$ and repelling for $\rho < 1$. Figure 3 shows the numerically computed footprint for this system at $\gamma = -0.01325$ and a range of ν. For the case $\gamma = -0.01324$ and $\nu = 0$ this is very close to resonance for the natural measure; the Lyapunov exponents for this measure are given by the crosses in the diagram.

The footprint of transverse Lyapunov exponents for the cycling Lorenz saddles is never contained within one quadrant as was the case in [1]. This is due to the presence of a non-trivial intersection of the chaotic saddles. More precisely $(\tilde{\lambda}, \tilde{\lambda})$ in the positive quadrant (off the scale in Figure 3) is in the footprint simply because there is a Dirac measure at the origin common to all A_i. As a consequence, the set of connecting orbits C_{12} that consist of points in $N_{12} \setminus (S_1 \cup S_2)$ whose ω and α limits are contained in $S_1 \cup S_2$ will not consist purely of a closed set of trajectories from S_1 to S_2; the cycle is *dirty* in the terminology of [1].
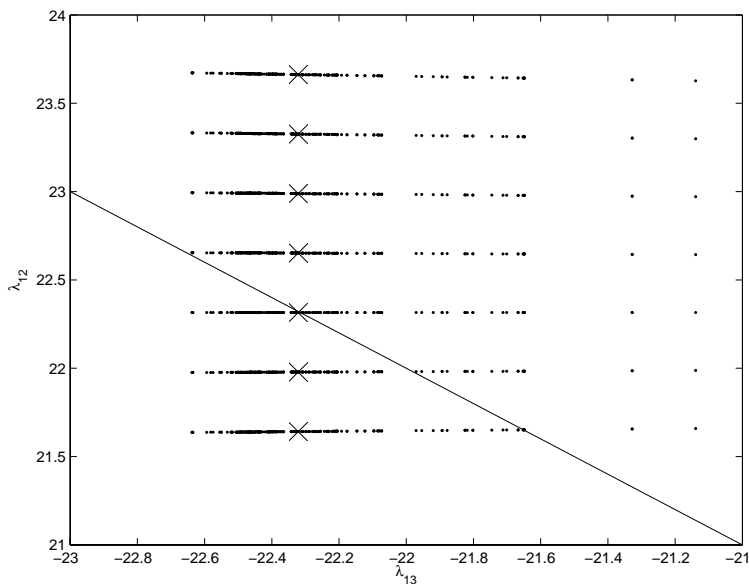
7

Figure 3: The footprint of transverse Lyapunov exponents $(\lambda_{13}, \lambda_{12})$ for the coupled Lorenz systems with $\gamma = -0.01325$ and a range of ν; from bottom to top the footprint is given starting at $\nu = -0.0002$ and increasing in steps of 0.0001. The Lyapunov exponent for the natural measure is at the point marked by the cross. The $\lambda_{12} = -\lambda_{13}$ line is shown and there is attracting cycling chaos when the cross lies below this line. The footprint is the form of a line rather than a region with polygonal boundary because the dependencies of the Lyapunov exponents on $\mathbf{x}_1(t)$ are identical.

2.2 Numerical loss of coherence and phase-resetting

As discussed in [3, 4], a cycle with only one trajectory in the connections between saddle equilibria will mean that connecting trajectories reset to asymptotically the same value on entering a saddle. This means that we observe identical segments of trajectory during the active phases. For the system here, we do not have this as the saddles are chaotic, however, in the special case that $\nu = 0$, trajectories appear to follow identical paths (see Figure 2) due to the skew product form of the coupling; we refer to this as 'false phase-resetting'.

Before breaking the skew product structure by setting $\nu \neq 0$, we discuss the issue of numerical loss of coherence. Just as chaotic systems do not permit their full trajectories to be computed numerically without loss of precision from their initial conditions, so in this system of coupled Lorenz systems we cannot expect to see periodic orbits of arbitrarily long period, or expect phase setting of active trajectory segments to persist for arbitrarily long phases of an attracting cycle. Instead, sensitive dependence on initial conditions within the chaotic saddle means that by the time numerical round-off errors have grown to a significant size, we may be shadowing a number of different trajectories. We called this effect *numerical loss of coherence* in [4].

This effect is present in the system (1). The effective time horizon can be estimated as $T^* \sim -\log(\eta)/\lambda_+$ where η is the machine accuracy and λ_+ is the most positive internal Lyapunov exponent. For the Lorenz equations with the given parameters this exponent is $\lambda_+ \approx 1.433$, and so for double precision machine accuracy ($\eta = 10^{-14}$) we can only expect periodic orbits of up to length $T^* \approx 22$. Figure 4 demonstrates this loss of coherence in a graphical representation used repeatedly in this paper. A single trajectory for the system is computed. Each time a $n_i = |\mathbf{x}_i|$ passes through 10^{-10} with $\dot{n}_i > 0$ we set T to zero and the segment of trajectory is plotted until the next $|\mathbf{x}_j|$ grows through 10^{-10}. This method superimposes each active phase of the trajectory on the previous ones. A circle is plotted as each segment ends so that the relative lengths of the collections of trajectory segments can be compared.

In Figure 4 we have set $\gamma = -0.0131$, a parameter at which periodic orbits might be expected (since $\rho < 1$). The identical length of successive trajectory segments concurs with this, although the trajectory is not periodic as the natural period of the system is longer than T^*, with successive trajectories losing coherence at around $T^* = 22$. Note that in Figure 2(a) and (b) the length of the phases shown and the period of the periodic orbit (respectively) are less than T^* and so we can observe the phase-resetting phenomenon. We note that plotting Figure 2(a) for a longer time series shows evidence of a numerical loss of coherence.

When we break this skew product structure by setting $\nu \neq 0$, we obtain attracting cycling chaos without phase-resetting at the same parameter values as Figure 2(a). The trajectory slows down as before but now after starting each active phase in the same way it diverges after a time significantly less than T^*.

Figure 5 shows trajectory segments plotted in the same way as Figure 4. Fifteen trajectory segments are shown in each plot. In each plot $\gamma = -0.014$, and the trajectory segments get successively longer, as the trajectory approaches the attracting cycle. The four plots show increasing
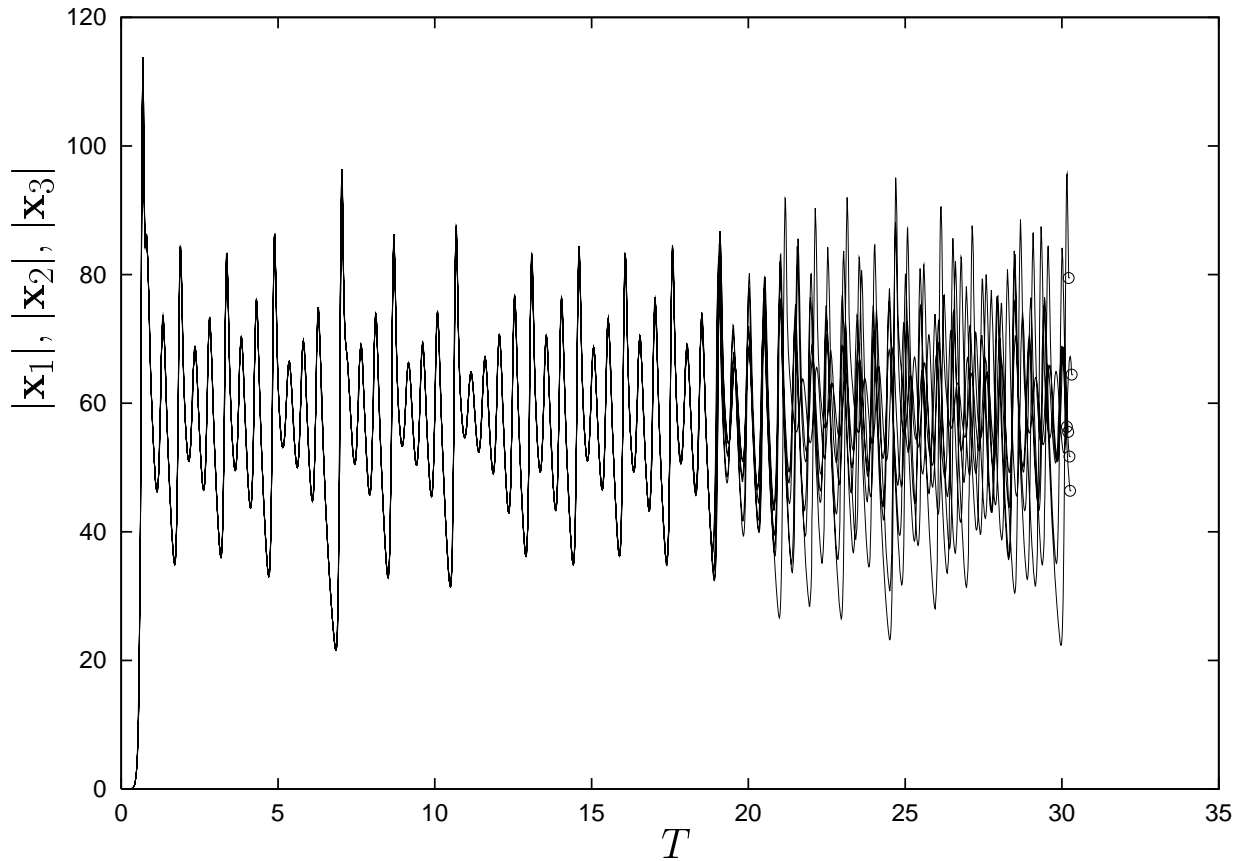
9

Figure 4: Numerical loss of coherence for the system 1 with $\nu = 0$. Each time an $n_i = |\mathbf{x}_i|$ passes through 10^{-10} with $\dot{n}_1 > 0$ we set $T = 0$ and the trajectory is plotted until the next $|\mathbf{x}_j|$ passes through 10^{-10}; the end of the segment is marked by a circle. Six successive segments of approach are shown here after transients have been resolved. The parameters are as before but with $\gamma = -0.0131$. Note that although the segments are all the same length, indicating periodic-type behavior, there is a loss of coherence after about $T^* = 22$ time units. This is to be expected due to the positive internal Lyapunov exponent of the Lorenz system overcoming finite machine precision.
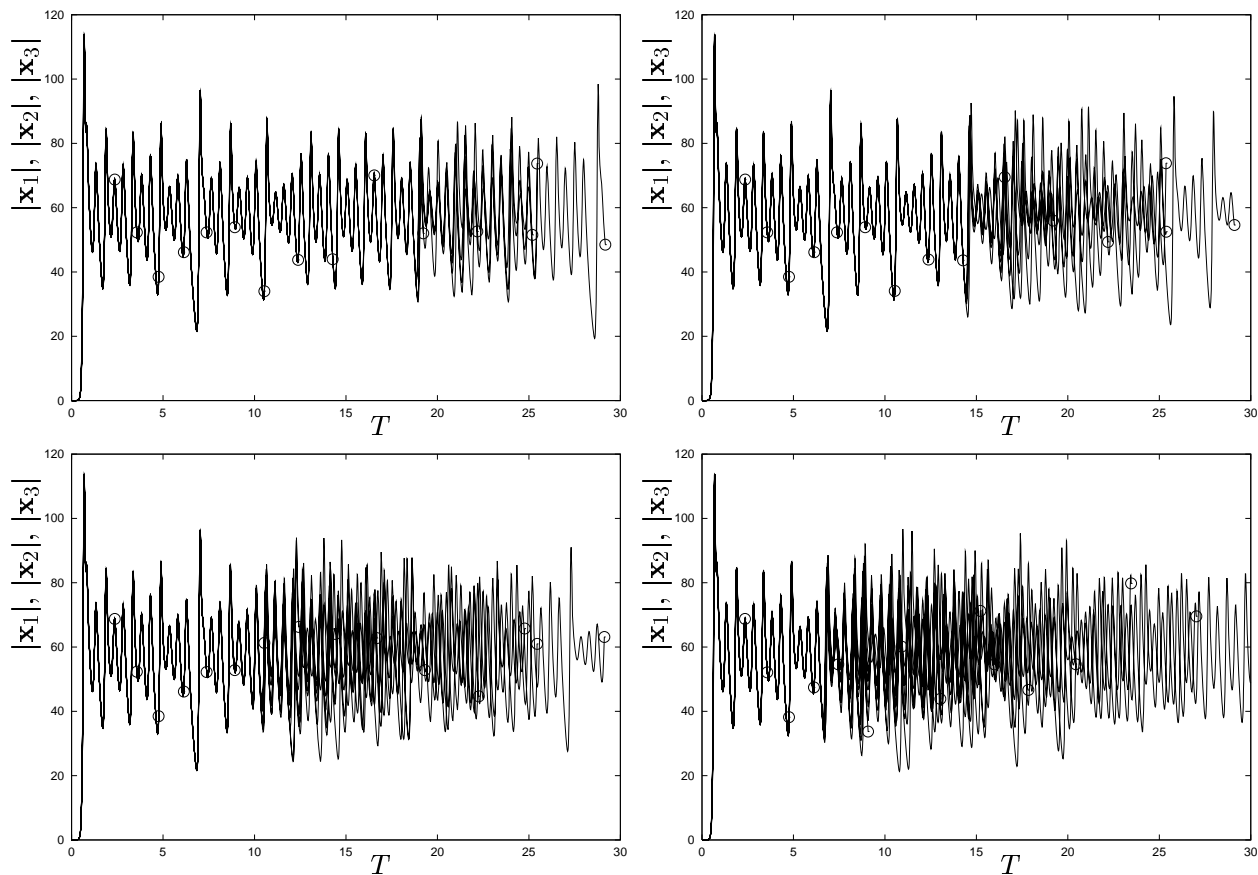
Figure 5: In (a) (top-left) $\nu = 0.0$, and again we see the numerical loss of coherence of the system at around $T^* = 22$. In (b) (c) and (d) $\nu = 10^{-12}$, 10^{-9}, 10^{-6} respectively, and the onset of loss of coherence T^* occurs at increasingly early times. The diagrams show repeated approaches to a chaotic saddle for the original system. As in Figure 4, each time an $|\mathbf{x}_i|$ passes through 10^{-10} we set T to zero and the trajectory is plotted until the next $|\mathbf{x}_j|$ passes through 10^{-10}; the end of the segment is marked by a circle. Fifteen successive trajectories are shown for different values of ν. In all pictures $\gamma = -0.014$, and the slowing down is reflected in the fact that the segments get successively longer.
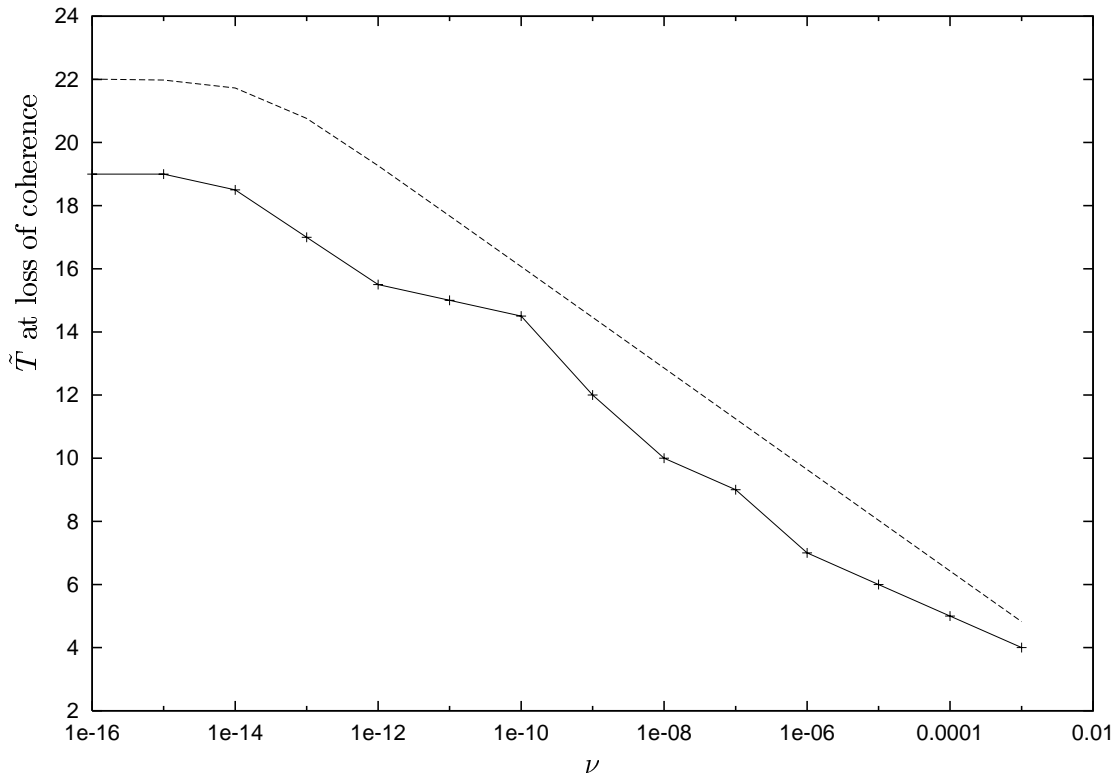
11

Figure 6: The time $\tilde{T}$ of loss of coherence as a function of ν. The dotted line is $\tilde{T} = -(\log|\nu| + |\eta|)/\lambda_+$. The solid line takes values of $\tilde{T}$ from time series such as in Figure 5. Note the saturation at $\tilde{T} = T^*$ when ν reaches machine precision.

values of ν. In (a), $\nu = 0$, and the phase-resetting is complete up to the point at which numerical loss of coherence causes the trajectory segments to separate (as in Figure 4). Figures (b), (c) and (d) show $\nu = 10^{-12}$, 10^{-9}, 10^{-6} respectively. The onset of loss of coherence occurs earlier as ν increases.

Similar to the computation of T^* above, the time $\hat{T}$ at which the skew-product-breaking term causes the separation of trajectory segments is given by $\hat{T} \sim -\log(\nu)/\lambda_+$ (recall λ_+ is the most positive internal Lyapunov exponent). For small values of ν the numerical loss of coherence in the system begins to dominate this agreement. We combine the two estimates to give the time at which loss of coherence occurs:

$$\tilde{T} = T^* + \hat{T} \sim -\frac{\log(|\nu| + |\eta|)}{\lambda_+}.$$

This line is plotted in Figure 6 (dotted line), along with (solid line) values of $\tilde{T}$ at which coherence is seen to be lost for different values of ν (this was obtained from time series like Figure 5, spotting $\tilde{T}$ by eye).

2.3 Absence of anomalous connections

Although the saddles A_i all contain the origin (and hence there are connecting orbits that do not follow the order $A_1 \mapsto A_2 \mapsto A_3 \mapsto A_1$) in practice we never see *anomalous switches* caused by close approaches to $0 \in A_i$. We explain this by reference to the expected recurrence times to a neighborhood of the origin within the attractor.

We can estimate the likely distance of closest approach of a trajectory to 0 as follows. Let $1/\delta$ be the dimension at 0 of the natural measure μ on A_i ($\delta > 1/3$); then the measure of a ball of radius ϵ about 0 will scale as: $\mu(B_\epsilon(0)) \sim \tilde{C}\epsilon^{1/\delta}$. Therefore, if $\epsilon(T)$ is the distance of closest approach to 0 of some typical trajectory approaching A_i as time T progresses, then we expect $\epsilon(T) \sim C_1 T^{-\delta}$. Observe that $C_1 > 0$ is constant on each visit to an A_i, and is constant throughout the trajectory for the phase resetting case. By contrast, the decaying variable near A_i will be of the form $C_2 e^{\lambda_{13}T}$ with $\lambda_{13} < 0$. Thus an anomalous switch on an approaching trajectory can occur only if

$$C_1 T^{-\delta} < C_2 e^{\lambda_{13}T}.$$

This implies that anomalous switches become ever more unlikely as approach to the cycle continues; the only circumstances in which we expect them to appear is for phase-resetting cycling when the connection comes close to being a homoclinic connection to the origin.

2.4 Bifurcation diagram and approximation of periodic orbits

In this section we give more numerical details of the structure of parameter space for the system (1). Figure 7 is a bifurcation diagram showing periodic, non-periodic and slowing down behaviors. The resonance bifurcation as a function of γ and ν is plotted by computing the transverse Lyapunov exponents λ_{12} and λ_{13} for different parameters (recall that the resonance occurs when $\rho = |\lambda_{12}/\lambda_{13}| = 1$). The black solid line shows where $\rho = 1$. The position of the resonance bifurcation depends roughly linearly on ν in this diagram.

We plot the bifurcation diagram by computing trajectories for different parameter values. For fixed parameters, we compute a long trajectory and record the lengths l_i of successive segments defined as before to begin when one $|\mathbf{x}_i|$ grows through 10^{-10} and to end when the next $|\mathbf{x}_j|$ grows through this point. Then we compute the ratio $\tau_k = l_k/l_{k-1}$; for a periodic orbit we expect τ_k to approach unity for large k, whereas for non-periodic behavior (stuck-on chaos in the terminology of [1, 3]), τ_k fluctuates around unity. Finally, if any of the $|\mathbf{x}_i|$ gets too close to an invariant subspace, (here within 10^{-320}) it becomes numerically stuck in that subspace ($|\mathbf{x}_i| = 0$ for all time) and the numerics become unreliable beyond this point. This case corresponds to the trajectory being attracted to a stable cycle (and thus eventually approaches too close to an invariant subspace), or to a very long periodic orbit which goes too close to an invariant subspace.

In Figure 7, to the left of the resonance line all points are grey, indicating the expected cycling chaos. Grey points also encroach on the right side of the resonance line (the 'non-cycling' side), indicating very long periodic orbits (or stuck-on chaos) which accumulate on the cycling. Further

to the right, trajectories no longer get numerically stuck in invariant subspaces and we see a region of coexisting periodic orbits and non-periodic behavior. Observe however that for the degenerate case $\nu = 0$ the 'false phase resetting' effect gives a line of periodic orbits in (γ, ν) space. Further from resonance there are regions where all trajectories are periodic, or non-periodic. These regions intermingle with each other in a complicated manner.

3   A mapping model from magnetoconvection

We now turn to a second example of cycling chaos; in this case, phase resetting effects are genuine, and we are able to demonstrate the creation of an infinite number of stable periodic orbits at resonance, as observed in [3] for a different system and conjectured by [2] for this system.

In [2], nonlinear 3D magnetoconvection in a certain limit was modeled using a set of ninth-order truncated ordinary differential equations (ODEs). The system has symmetries which force the presence of invariant subspaces; in particular there are a number of invariant subspaces given by P_x and P_y within which are chaotic invariant sets A_x and A_y respectively and an attracting heteroclinic cycle between these two chaotic sets and two fixed points may exist and be robust for some region in parameter space (we refer to [2] for more details). This differs from the Lorenz equations example considered above in that the cycle sequentially visits equilibrium points and chaotic sets. When such a cycle loses transverse stability via a resonance bifurcation, a series of high period periodic attractors are created, such that the periods of these periodic orbits appear to accumulate at the resonance.

To study further the phenomena in the ODEs, the system was reduced in [2] to the following approximate return map to a neighborhood of one of the equilibria, and we consider the appearance of cycling chaos within the dynamics of this map.

3.1   The magnetoconvection map

The map is defined on the phase space

$$\{(x_0, x_2, y_0, y_2) \in \mathbb{R}^4 \ : \ |x_2| = 1 \text{ or } |y_2| = 1 \text{ and } x_0, y_0 \text{ are small.}\}$$

as a piecewise smooth function; this definition comprises four parts. Near the invariant subspace P_x corresponding to $x_2 = \pm 1$ the evolution of x_0 is governed by the Lorenz map, y_0 undergoes roughly linear growth and y_2 undergoes roughly linear decay:

$$(x_0, x_2 = \pm 1, y_0, y_2) \to (\text{sgn}(x_0)(-\kappa + C_1|x_0|^{\delta_1}), -x_2, C_2 y_0|x_0|^{\delta_2}, C_3 y_2|x_0|^{\delta_3}). \tag{7}$$

The exponents δ_2 and δ_3 are such that the average values of $|x_0|^{\delta_2}$ and $|x_0|^{\delta_3}$ are greater and less than one, respectively. This map is valid while $|x_0| > |y_0|$. As soon as this inequality is violated, we have a *switch map*, which takes the trajectory close to P_y:

$$(x_0, x_2 = \pm 1, y_0, y_2) \to (C_4 x_0|y_2|^{\delta_4}|y_0|^{\delta_2}, \pm C_5|y_2|^{\delta_5}|y_0|^{\delta_3}, \text{sgn}(y_0)(-\kappa + C_6|y_2|^{\delta_6}|y_0|^{\delta_1}), \text{sgn}(y_2)). \tag{8}$$
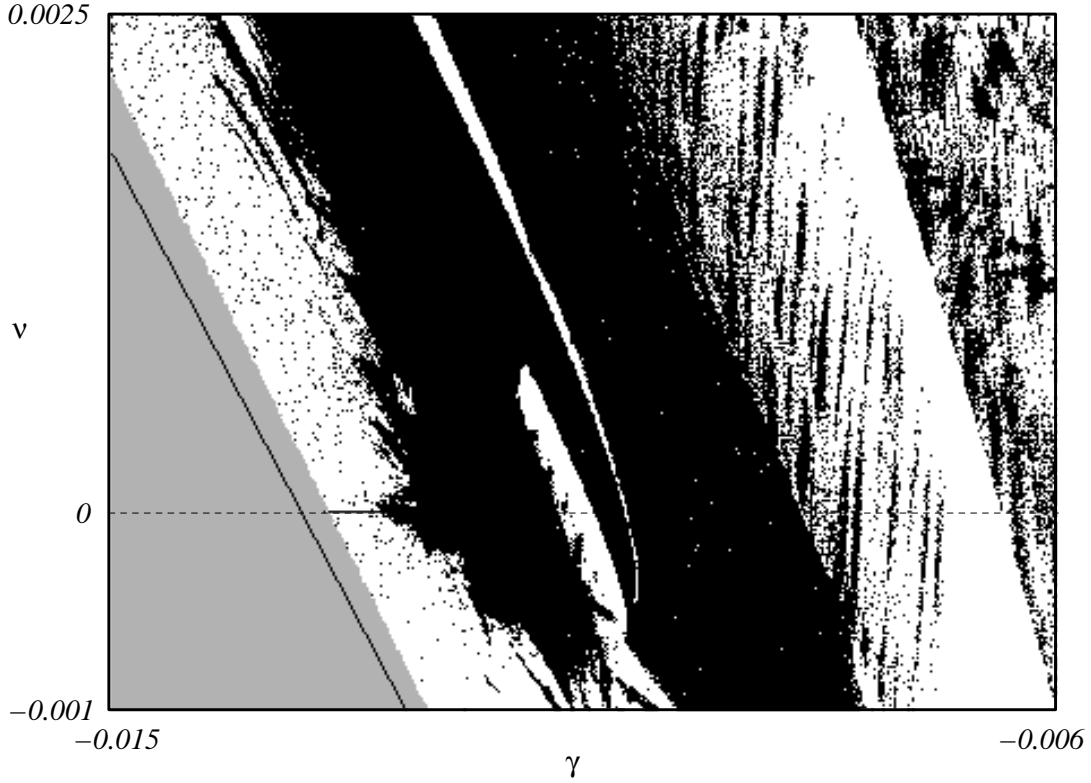
Figure 7: Bifurcation diagram of periodic orbits, stuck-on chaos and cycling chaos. Black points indicate periodic orbits, where $|\tau_{100} - 1|$, $|\tau_{99} - 1|$, $|\tau_{98} - 1| < 0.01$ (see text for definition of τ). White points represent non-periodic behavior (stuck-on chaos), where $|\tau_{100} - 1|$ or $|\tau_{99} - 1|$ or $|\tau_{98} - 1| \geq 0.01$. Grey points indicate cycling chaos or very long periodic orbits, where the trajectory is numerically rounded into an invariant subspace ($|\mathbf{x}_i| = 0$). The solid black line marks the resonance bifurcation and the dashed line is $\nu = 0$. The initial conditions used were $(\mathbf{x}_1, \mathbf{x}_2, \mathbf{x}_3) = (0.1, 0.2, 0.3, 10^{-10}, 2 \times 10^{-10}, 3 \times 10^{-10}, 3 \times 10^{-20}, 2 \times 10^{-20}, 10^{-20})$ and periodic orbits were examined after a transient was computed.

15

The next component is equivalent to (7) (up to a relabelling), and y_0 has Lorenz map dynamics, while x_0 and x_2 grow and decay respectively:

$$(x_0, x_2, y_0, y_2 = \pm 1) \to (C_2 x_0 |y_0|^{\delta_2}, C_3 x_2 |y_0|^{\delta_3}, \text{sgn}(y_0)(-\kappa + C_1 |y_0|^{\delta_1}), -y_2). \qquad (9)$$

Similarly, this map continues until $|y_0| \leq |x_0|$ when we apply another switch map back to P_x:

$$(x_0, x_2, y_0, y_2 = \pm 1) \to (\text{sgn}(x_0)(-\kappa + C_6 |x_2|^{\delta_6} |x_0|^{\delta_1}), \text{sgn}(x_2), C_4 y_0 |x_2|^{\delta_4} |x_0|^{\delta_2}, \pm C_5 |x_2|^{\delta_5} |x_0|^{\delta_3}).$$
$$(10)$$

From fitting the dynamics of the map to the ODEs, values for the constants and the eigenvalues depending on a bifurcation parameter β are given in [2]. Note that this system is extremely sensitive with respect to parameter values, and so we give these to precisely the same number of decimal places as are used in our (double precision) numerical computations. The δ exponents are determined from solutions of the ODE:

$$\delta_1 = \frac{-\lambda_\zeta}{\mu}(1 + \delta_6) \quad \delta_2 = \frac{-\lambda_\zeta}{\mu}\delta_4 - 1 \quad \delta_3 = \frac{-\lambda_\zeta}{\mu}(1 + \delta_5)$$
$$\delta_4 = \frac{\beta\mu}{\lambda^+} \qquad\qquad \delta_5 = \frac{\lambda_\zeta}{\lambda^+} \qquad\qquad \delta_6 = \frac{-\lambda_2^-}{\lambda^+}$$

where the eigenvalues λ_ζ, λ^+ and λ_2^- are computed from the ODEs as:

$$\lambda_\zeta = -0.059697 \quad \lambda^+ = 0.29606 \quad \lambda_2^- = -0.048978.$$

Finally the constants are given by

$$C_1 = -0.12449854, \quad C_2 = 0.27199631, \quad C_3 = 0.16791468$$
$$C_4 = 609.64770, \quad C_5 = 0.86514592, \quad C_6 = 0.0015973505$$
$$\kappa = -0.014072345, \quad \mu = 0.1655.$$

Just as in [2, 3] we iterate the map in logarithmic coordinates in order to resolve the large dynamic range of the variables.

3.2 Bifurcation diagram

This model exhibits a plethora of periodic orbits whose periods appear to accumulate as the resonance bifurcation is approached, as discussed in [2]. These periodic orbits appear to have interesting basins of attraction; Figure 8 shows an example of a numerically obtained bifurcation diagram. We iterate the map with a grid of initial conditions in $\log|y_0|$ and $\log|y_2|$ (here $\beta = 1.089$, and we plot different shades to represent the different periods of periodic orbits. All initial conditions shaded in the grey region on the right of the figure finish up at periodic orbits of period 102 (plotted as the furthest top-right black circle on the figure. Note that the periodic orbits of period 102 are not all absolutely identical, but are the same to one or two decimal places. Other periods plotted here are 232, 344, 410, 460, in other shades of grey. The basins shown in Figure 8 are only a small part of a much more complicated picture — periodic orbits for other periods exist and the full basin diagram has many intermingled basins. Note that the periodic orbits lie on a straight line in $\log|y_0|$-$\log|y_2|$
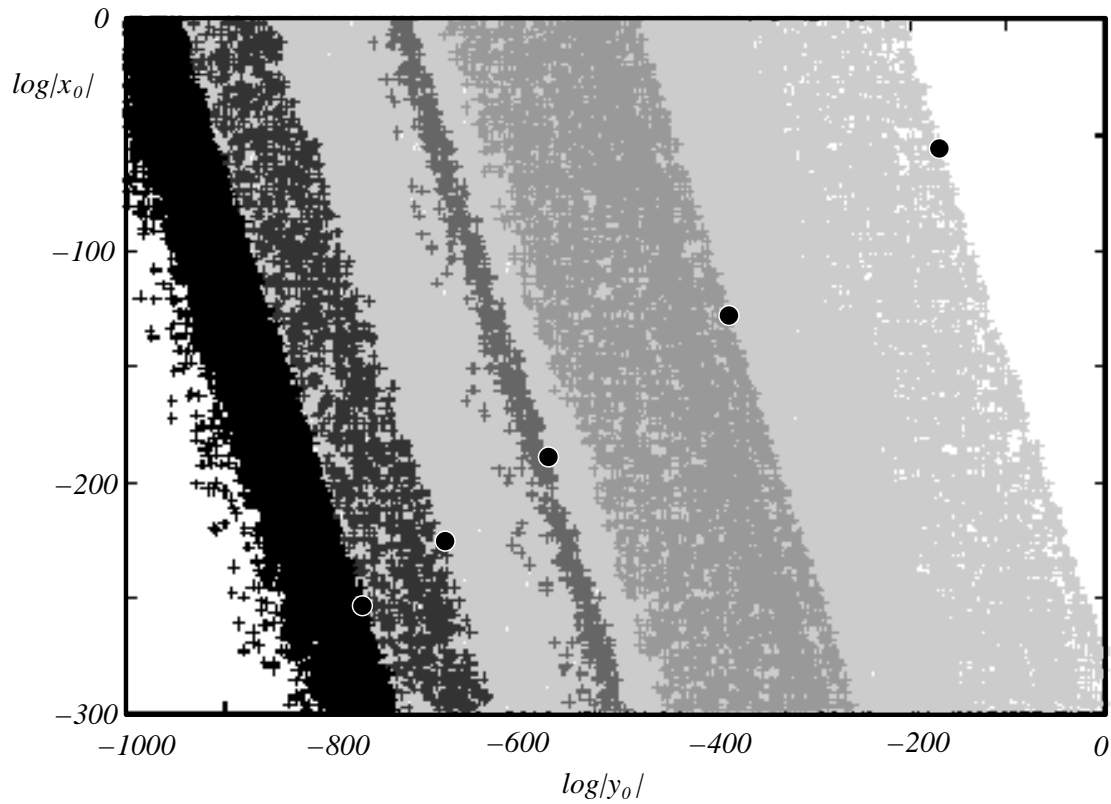
16

Figure 8: Basin of attraction for different periodic orbits, with $\beta = 1.089$. The map is iterated with different initial values of $\log|y_0|$ (horizontal axis) and $\log|y_2|$ (vertical axis). Initial conditions leading to periodic orbits of period 102 are plotted in grey in the rightmost region. The period-102 orbit lie clustered around the top right black circle, on the edge of the basin boundary. Four other periods (232, 344, 410, 460) are represented by increasingly dark shades, together with black dots representing the periodic orbits that appear to be close to the edges of their basins of attraction. White in the top right corner means that trajectories escape, while white in the bottom left corner indicate that trajectories mainly go to even longer periodic orbits.
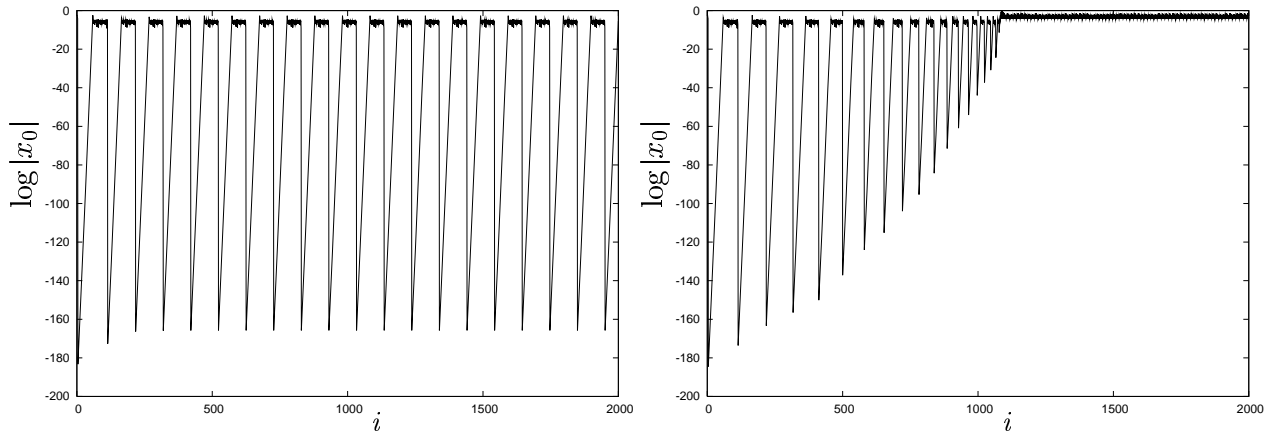
Figure 9: Time series showing the fragility of periodic orbits in the magnetoconvection model. Figure (a) has an initial value $y_2^{(0)} = 10^{-300}$ and there is an attracting periodic orbit. Figure (b) has identical parameters and initial conditions but now the initial $y_2^{(0)} = 10^{-302}$, resulting in the periodic orbit being attracted to a low period periodic orbit far from the invariant subspaces.

space, and the striped basin boundaries. The presence of a scattering of white throughout most of the basins, especially to the right of the figure, suggests that their basins are pseudo-riddled [10].

Because of the pseudo-riddled nature of the basins of attraction, these periodic orbits appear are fragile in the sense that altering parameters, initial conditions or perturbing the model very slightly can cause a trajectory close to a periodic orbit to leave the vicinity of the invariant subspaces and tend to a low period attracting state as illustrated in Figure 9. Each plot shows a time series of $\log |x_0|$ for the fixed parameters above, and $\beta = 1.088$. Three initial conditions are fixed as $(x_0^{(0)}, x_2^{(0)}, y_0^{(0)}) = (\kappa + 1, 1, 10^{-2.5})$. Figure 9(a) has $y_2^{(0)} = 10^{-300}$ and this initial condition leads to a stable periodic orbit. Figure 9(b) is for the same system, but now has $y_2^{(0)} = 10^{-302}$. Here convergence to the periodic orbit is not found and the trajectory leaves the vicinity of the invariant subspaces. A similar effect can be observed by incorporating a small perturbation e.g. to κ.

3.3 Constructing approximate periodic orbits

The map exhibits a form of 'phase-resetting' due to the fact that the x_0 or y_0 variable always starts at $-\kappa$ for any connecting orbit, since for any such orbit $y_2 = 0$ initially. This corresponds to starting on the unstable manifold of an equilibrium point in the original ODEs. As found in [3], resonance near a phase-resetting cycle can result in creation of a large number of stable periodic orbits. For the remainder of this section we aim to construct these periodic orbits near resonance. This gives some insight as to why there are so many simultaneously stable periodic orbits in Figure 8.

We follow the method of [3] and use Figure 10 as a guide. In this figure we plot only half a period and assume that the two halves are identical up to a relabelling. More precisely, we assume that at $i = 0$, we have just made one iterate of map (10), resetting so that we are close to the P_x subspace. Thus we have initial values $\log |x_0^{(0)}| = \log |\kappa|$ (this is taken to be exact as we need 'phase-resetting'
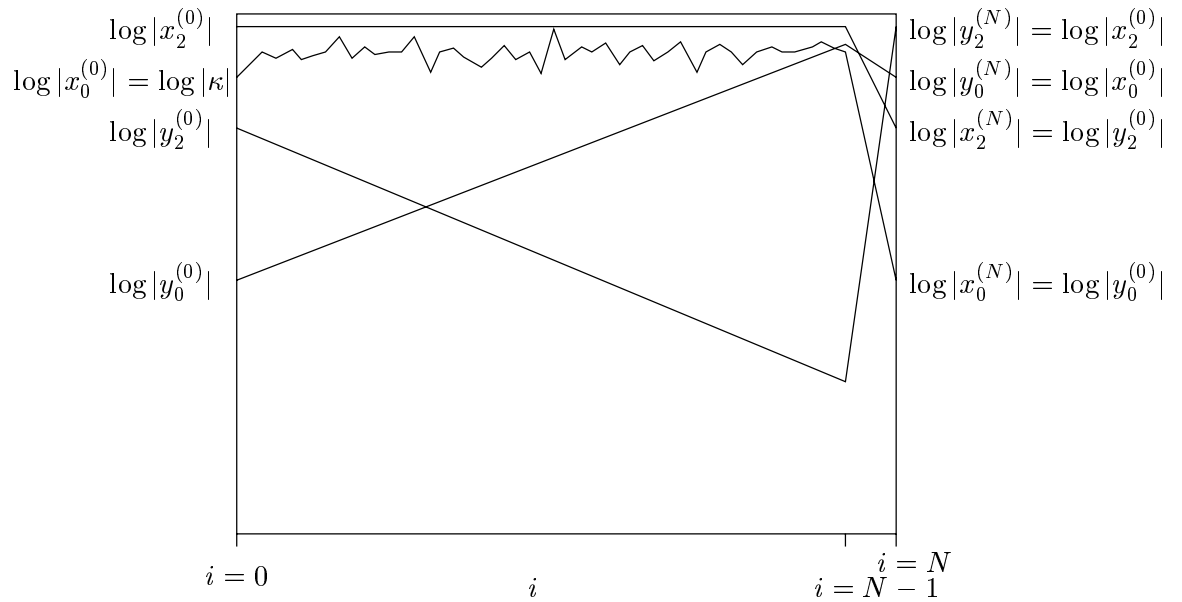
18

Figure 10: Schematic diagram of half a periodic orbit for the map (7-10). There are $N-1$ iterates of map (7) followed by a single iterate of map (8). By matching the final and initial states we can construct an approximation to a long-period orbit of the map.

for periodic orbits to appear), $\log|x_2^{(0)}| = 0$, $\log|y_0^{(0)}|$ and $\log|y_2^{(0)}|$. There follow $N-1$ iterates of map (7), during which time $\log|y_0|$ grows and $\log|y_2|$ decays (but roughly linearly), whilst x_0 undergoes iterates of the Lorenz map, and $\log|x_2|$ remains at zero. After $N-1$ iterates we assume $\log|y_0|$ has grown sufficiently so that $\log|y_0^{(N-1)}| > \log|x_0^{(N-1)}|$, and then a switch occurs, in the form of a single iterate of map (8). If we assume the two halves of a periodic orbit are identical, then we should find (after relabelling)

$$\begin{aligned} \log|x_0^{(N)}| &= \log|y_0^{(0)}| \\ \log|x_2^{(N)}| &= \log|y_2^{(0)}| \\ \log|y_0^{(N)}| &= \log|x_0^{(0)}| = \log|\kappa| \\ \log|y_2^{(N)}| &= \log|x_2^{(0)}| = 0. \end{aligned}$$

For a periodic orbit we wish to find $\log|y_0^{(N-2)}|$ and $\log|y_0^{(N-1)}|$ such that

$$\log|y_0^{(N-2)}| < \log|x_0^{(N-2)}| = \log|f^{(N-2)}(\kappa)|,$$

and $\log|y_0^{(N-1)}| > \log|x_0^{(N-1)}| = \log|f^{(N-1)}(\kappa)|$ (i.e. we assume a switch occurs at precisely the $(N-1)$th iterate). Here $f^{(j)}$ represents the jth iterate of the Lorenz map. Whilst iterating map (7) we use $y_0 \to C_2 y_0 |x_0|^{\delta_2}$ which in logarithmic coordinates is

$$\log|y_0| \to \log|y_0| + \log(C_2) + \delta_2 \log|x_0|.$$

Hence after k iterations we have

$$\log|y_0^{(k)}| = \log|y_0^{(0)}| + k(\log|C_2| + \delta_2 A_k)$$

19

where $A_n = \frac{1}{n} \sum_{j=0}^{n-1} \log |f^{(j)}(\kappa)|$. Now $\log |y_0^{(0)}| = \log |x_0^{(N)}|$ for a periodic orbit. Observe that $\log |x_0^{(N)}|$ is computed from one iterate of map (8): $x_0 \to C_4 x_0 |y_2|^{\delta_4} |y_0|^{\delta_2}$ so that

$$\log |y_0^{(0)}| = \log |x_0^{(N)}| = \log |C_4| + \log |x_0^{(N-1)}| + \delta_4 \log |y_2^{(N-1)}| + \delta_2 \log |y_0^{(N-1)}|$$

giving

$$\log |y_0^{(k)}| = \log |C_4| + \log |x_0^{(N-1)}| + \delta_4 \log |y_2^{(N-1)}| + \delta_2 \log |y_0^{(N-1)}| + k(\log |C_2| + \delta_2 A_k). \qquad (11)$$

Similarly,

$$\log |y_2^{(N-1)}| = \log |y_2^{(0)}| + (N-1)(\log |C_3| + \delta_3 A_{N-1})$$

and

$$\log |y_2^{(0)}| = \log |x_2^{(N)}| = \log |C_5| + \delta_5 \log |y_2^{(N-1)}| + \delta_3 \log |y_0^{(N-1)}|$$

after one iterate of map (8). Combining these two expressions gives:

$$\log |y_2^{(N-1)}| = \log |C_5| + \delta_5 \log |y_2^{(N-1)}| + \delta_3 \log |y_0^{(N-1)}| + (N-1)(\log |C_3| + \delta_3 A_{N-1})$$

and after rearranging we get

$$\log |y_2^{(N-1)}| = \frac{(N-1)(\log |C_3| + \delta_3 A_{N-1}) + \log |C_5| + \delta_3 \log |y_0^{(N-1)}|}{1 - \delta_5}.$$

Substituting this into (11) gives

$$\log |y_0^{(k)}| = \log |C_4| + \log |x_0^{(N-1)}| + \delta_2 \log |y_0^{(N-1)}| + k(\log |C_2| + \delta_2 A_k)$$
$$+ \delta_4 \frac{(N-1)(\log |C_3| + \delta_3 A_{N-1}) + \log |C_5| + \delta_3 \log |y_0^{(N-1)}|}{1 - \delta_5}.$$

Setting $k = N - 1$ now enables us to extract an expression for $\log |y_0^{(N-1)}|$:

$$\log |y_0^{(N-1)}| = \Big[(1 - \delta_5)(\log |C_4| + \log |x_0^{(N-1)}| + (N-1)(\log |C_2| + \delta_2 A_{N-1})) +$$
$$\delta_4((N-1)(\log |C_3| + \delta_3 A_{N-1}) + \log |C_5|)\Big] / \big[(1 - \delta_5)(1 - \delta_2) - \delta_3 \delta_4\big]$$

and this can be substituted into (12) with $k = N - 2$ to obtain an expression for $\log |y_0^{(N-2)}|$. Both expressions are long, but simply rely on being able to compute N iterates of the Lorenz map. Each are computed numerically, and compared with iterates of $f^{(N)}(\kappa)$ (exactly the same N iterates of the Lorenz map). In a similar way to [3] we look for values of N which are good candidates for a periodic orbit. In this case, this means values of N for which $\log |y_0^{(N-2)}| < \log |f^{(N-2)}(\kappa)|$ and $\log |y_0^{(N-1)}| > \log |f^{(N-1)}(\kappa)|$. Our expressions for $\log |y_0^{(N-2)}|$ and $\log |y_0^{(N-1)}|$ can be simplified further by replacing both the $(N-1)$-average A_{N-1}, and the $(N-1)$th iterate $\log |x_0^{(N-1)}|$ with the long-term (ergodic) average A_∞. This leads to straight line equations for both $\log |y_0^{(N-2)}|$ and $\log |y_0^{(N-1)}|$ with gradients and intercepts that are functions only of β.

3.4 Computing a bifurcation diagram

Figure 11 shows the curves of $\log|y_0^{(N-2)}|$ (dark) and $\log|y_0^{(N-1)}|$ (light) for three values of β: (a) $\beta = 1.0887 < \beta_c$, (b) $\beta = 1.0896 = \beta_c$, (c) $\beta = 1.091 > \beta_c$. Also plotted are the Lorenz iterates $\log|f^{(N-1)}(\kappa)|$ (black), together with the straight line approximations to the curves (black solid and dashed lines). We expect a periodic orbit whenever the black curve is between the light and dark grey curves. As in [3], for $\beta < \beta_c$, the overall positive gradient of the two curves takes them away from the Lorenz iterates after some crossings, here near $N = 1000$, indicating that we may expect periodic orbits of period around 1000, but that much longer periodic orbits should not be expected. For $\beta = \beta_c$ there is no overall linear growth of the curves, but increasing chaotic fluctuations (driven by the NA_{N-1} term) ensure that we have repeated crossing of the Lorenz iterates, for arbitrarily high periods. For $\beta > \beta_c$ we have relatively short periodic orbits indicated before the negative gradient again takes the curves away from the Lorenz iterates.

Note that there is a difference between these figures and the corresponding ones in [3]; in that paper the curves begin below the threshold required to construct a return, and so we are guaranteed crossings on the 'periodic orbit' side of the resonance, and we are guaranteed to have none well beyond the resonance on the 'cycling' side. Here the opposite is true, so that far from resonance on the periodic side, no periodic orbits are indicated, whereas short periodic orbits on the cycling side are always indicated. This is in agreement with the numerically computed bifurcation diagram, in which a collection of short periodic orbits appear for all parameter values beyond the resonance, and suggests that the resonance bifurcation cycling chaos in this map is 'subcritical'.

A bifurcation diagram can be computed in the same way as in [3]; see Figure 12. For each value of β we compute the curves $\log|y_0^{(N-1)}|$ and $\log|y_0^{(N-2)}|$ and find values of N for which they lie on either side of $\log|f^{(N-1)}(\kappa)|$. These points are plotted as grey dots. For comparison, actual periodic orbits found by iterating the full system with a grid of initial conditions is overlaid in dark points. The envelope containing the approximated periodic orbits is plotted as a solid black line, computed by finding the first and last crossings of the Lorenz iterates. This gives an approximation of the rate of approach to the accumulation of periods at resonance.

4 Discussion

In summary, we have returned to two systems in the literature that display robust attracting heteroclinic cycles between chaotic saddles. The first case is a ring of three coupled Lorenz systems from [7], the second is a mapping approximating a limiting case of 3D magnetoconvection from [2]. In both cases we give a detailed description and approximation of stable periodic orbits that appear near resonance, and investigate the structure of the basins of attraction of periodic orbits. For the coupled Lorenz system we discuss the appearance of false phase-resetting for the case $\nu = 0$. By introducing a bidirectional coupling we destroy the appearance of this false phase-resetting and can estimate the time to loss of phase coherence over successive approaches to the chaotic saddles. For the first system we also argue that although the chaotic saddles contain points of higher isotropy,

and because of this anomalous connections, the rate of approach to invariant subspaces is so fast that the anomalous connections will typically not be seen with the attractor.

By contrast, the magnetoconvection map exhibits genuine phase-resetting, owing to the presence of equilibria in the cycle, as investigated in [4, 5]. We suspect that generally speaking, cycling chaos between sets that include equilibria will contain the phase-resetting connections needed to see long-period periodic orbits close to resonance. In the absence of this we expect non-resetting connections and stuck-on chaos after resonance.

One might ask why cycling attractors have not been observed much in the literature. We tend to think that although such attractors are not very common, there may well be cases where they have been observed, but then dismissed as being 'too complicated'. We expect our ideas to be applicable to a range of examples, in particular to coupled cell systems, where there has been interest and observation of such attractors [12, 13]. Coupled cell systems appear naturally in a variety of contexts; an important example is model networks of coupled neurons which has motivated work observing heteroclinic cycles between cluster states; for example [6, 9]. One of the main obstructions to a good understanding of the dynamics of such high-dimensional coupled systems is the relative absence of a clear and useful classification of the attractors that one can typically find, and these systems are so complicated that a natural response is to abandon any attempt at a systematic understanding. Our results have opened up ways of analysing these kinds of systems, and the recognition that cycling chaos can occur in such systems is a significant step towards a better classification.

Finally, our investigations indicate that numerical simulation of these robust attractors is very difficult. Not only is careful choice of grid necessary to resolve the very small quantities to obtain correct qualitative behavior even for a relatively small time, but also the appearance of periodic orbits with complicated and as yet unexplained basin structure seems to be possible. In particular, the lack of any hyperbolicity of the cycling attractor as a whole means that appeals to the shadowing property for chaotic attractors will be in vain.

References

[1] P. Ashwin, Cycles homoclinic to chaotic sets; robustness and resonance. *Chaos* **7** 207–220 (1997).

[2] P. Ashwin and A. M. Rucklidge, Cycling chaos: its creation, persistence and loss of stability in a model of nonlinear magnetoconvection. *Physica D* **122** 134–154 (1998).

[3] P. Ashwin, A. M. Rucklidge and R. Sturman, Infinities of periodic orbits near robust cycling. *Phys. Rev. E* **66** 035201(R) (2002).

[4] P. Ashwin, M. Field, A. M. Rucklidge and R. Sturman, Phase resetting effects for robust cycles between chaotic sets. *Chaos* **13** 973–981 (2003).

[5] P. Ashwin, A. M. Rucklidge and R. Sturman, Two-state intermittency near a symmetric interaction of saddle-node and Hopf bifurcations: a case study from dynamo theory *Physica D* (2004), in press.

[6] P.L. Buono, M. Golubitsky and A. Palacios, Heteroclinic cycles in rings of coupled cells, *Physica D* **143** 74–108 (2000).

[7] M. Dellnitz, M. Field, M. Golubitsky, A. Hohmann and J. Ma, Cycling chaos *Intl. J. Bifurcation and Chaos* **5** 1243–1247 (1995).

[8] M. Field, *Lectures on Bifurcations, Dynamics and Symmetry*, Pitman Research Notes in Mathematics, Vol. 356 (1996).

[9] H. Kori and Y. Kuramoto, Slow switching in globally coupled oscillators: robustness and occurrence through delayed coupling. *Phys. Rev. E* **63** (2001), 046214;

[10] Y.-C. Lai, Pseudo-riddling in chaotic systems, *Physica D* **150** 1–13 (2001).

[11] E. Ott and J. Sommerer, Blowout bifurcations: the occurrence of riddled basins and on–off intermittency. *Phys. Lett. A* **188** 39–47 (1994).

[12] A. Palacios, Cycling chaos in one-dimensional coupled iterated maps. *Intl. J. Bifurcation and Chaos* **12** 1859–1868 (2002).

[13] A. Palacios and P. Longhini, Cycling behavior in near-identical cell systems. *Intl. J. Bifurcation and Chaos* **13** 2719–2732 (2003).
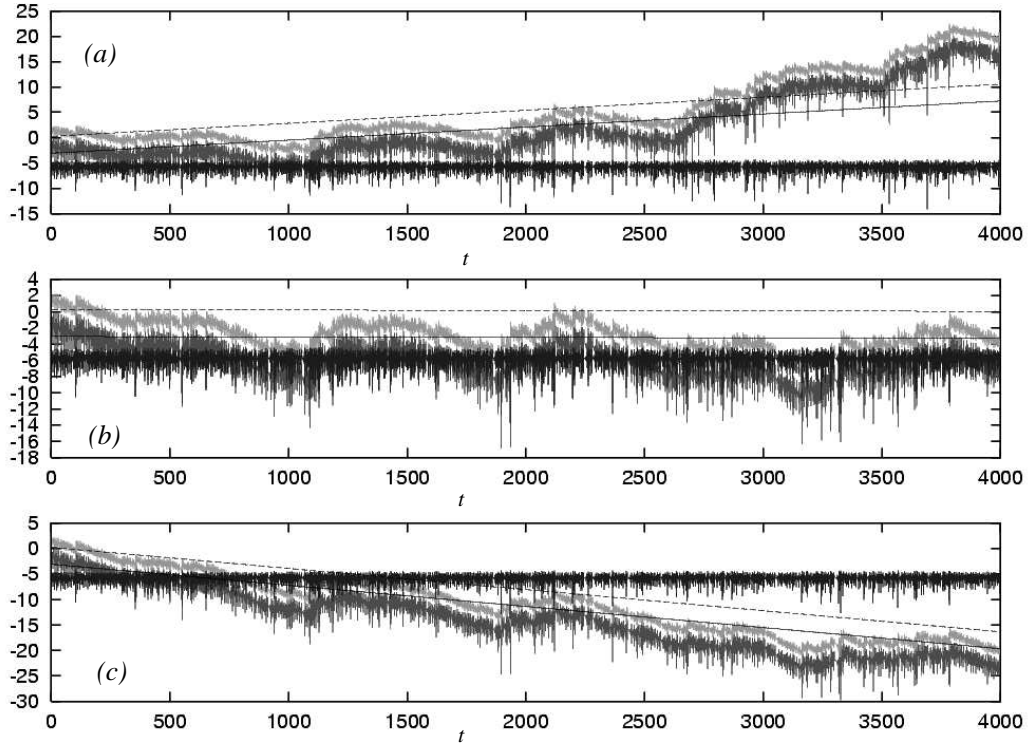
Figure 11: Three plots of $\log|y_0^{(N-2)}|$ (dark) and $\log|y_0^{(N-1)}|$ (light) crossing the chaotic evolution of $\log|f^{(N-1)}(\kappa)|$ (black). Solid and dotted lines indicate the linear approximations to these curves. Plot (a) is for $\beta < \beta_c$, and we have several crossings before the overall linear growth takes the curves away from the Lorenz iterates. Plot (b) is for $\beta = \beta_c$, for which there is no overall growth, and we get repeated crossings as the chaotic fluctuations of the curves increase. For (c) we have $\beta > \beta_c$ and we get relatively short periodic orbits indicated before the negative gradient again takes the curves away from the Lorenz iterates.
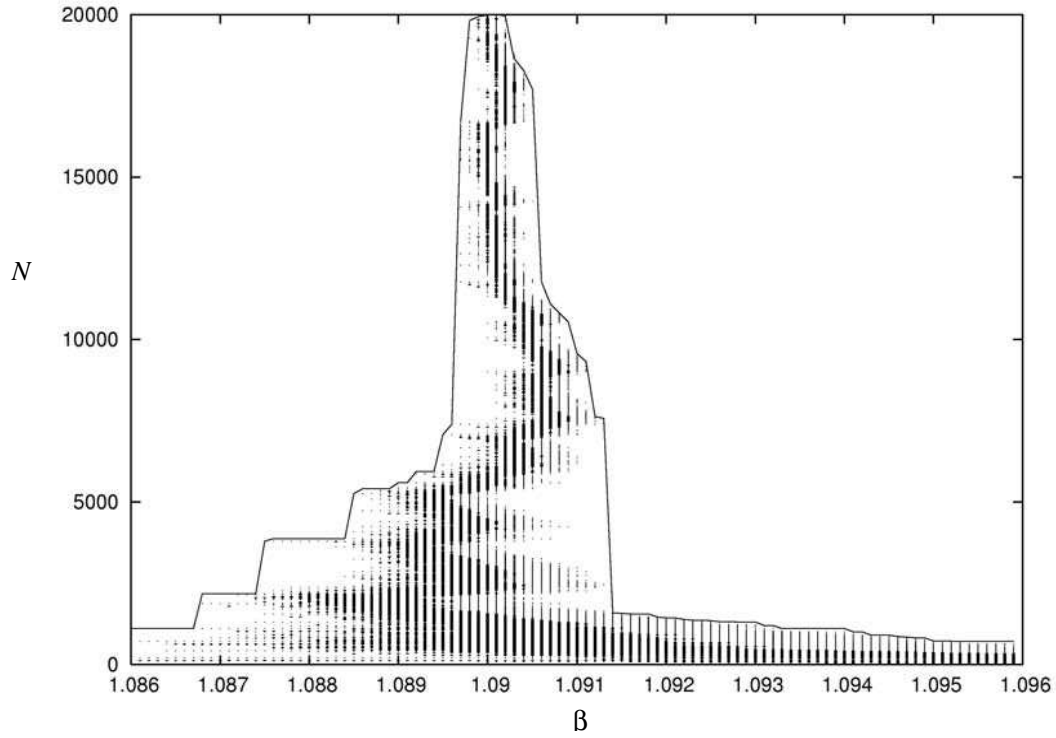
Figure 12: Bifurcation diagram of periodic orbits for the map (7-10) computed by constructing approximate periodic orbits as in Figure 11. The periods of the periodic orbits get longer as the resonance is approached (at $\beta_c = 1.0896$). Dots represent predicted periodic orbits, and the overlaid horizontal bars are actual periodic orbits. The black outlines are simply the envelope of the predicted dots (the first and last crossings of the curves), showing of accumulation of the periodic orbits as period $N \to \infty$.